Solid Oxide Fuel Cell Modeling with OpenFOAM®

Dong Hyup Jeon

Nomenclature

Cp	heat capacity, J/kg K
D	diffusivity, m^2/s
d_p	diameter of spherical particle, m
F	Faraday constant, 96,485 C/mol
ΔG°	gibb's free energy, J/kmol
H	enthalpy, J/kmol
i	current density, A/m^2
K	flow permeability, m^2
l	thickness, μm
M_i	molecular mass of gas species i, kg/mol
M_{ij}	mean molecular mass, kg/kmol
P	pressure, Pa
R_g	universal gas constant, 8.314 J/K mol
T	temperature, K or °C
u	velocity, m/s
V	voltage, V
V_i	diffusion volume of species i
x_i	mole fraction of component gas species i
y_i	mass fraction of component gas species i
	Greek Letters
ε	Porosity
η	overpotential, V
κ	thermal conductivity, W/m K

D. H. Jeon (✉)

Department of Mechanical System Engineering, Dongguk University-Gyeongju, Gyeongju 38066, Republic of Korea

e-mail: jeondh@dongguk.ac.kr

μ dynamic viscosity, Pa s
ρ density, kg/m^3
τ tortuosity

       Superscripts or Subscripts
0   initial
A   anode
act   activation
C   cathode
conc   concentration
eff   effective
H_2 hydrogen
H_2O water
O_2 Oxygen
T   total

1 Introduction

Solid oxide fuel cells (SOFCs) are an electrochemical device that converts the chemical energy stored in a variety of fuels directly into electricity and produces heat as its by-product. SOFCs typically operate in high temperature range (600–1000 °C) to achieve a good ionic conductivity of solid electrolyte. High temperature operation has advantages, such as high power efficiency, long-term stability, fuel flexibility and high temperature exhaust gas. This benefit further allows the system to be combined with gas turbine that can be an option for applications of auxiliary power unit of vehicles as well as industrial power supply. One the other hand, disadvantages include longer start-up time, thermal fatigue failure of the materials, sealing problem under high temperature, and mechanical and chemical compatibility issues. Therefore, the SOFCs operation within a tight design range is important (Hajimolana et al. 2011). In this respect, numerical modeling has become an attractive method for investigating the SOFCs that can optimize the cell parameters, decrease physical and chemical degradation, and finally improve its performance.

There are two principal SOFC configurations, e.g., tubular and planar. Typically, planar configuration consists of positive electrode/electrolyte/negative electrode (PEN) structure, gas channels and interconnects. Based on the component thickness, SOFCs are categorized to four types, e.g., anode-supported, electrolyte-supported, cathode-supported and metal-supported. When operating SOFCs, a fuel and an oxidant, supplied from gas channels, are introduced to the PEN structure. Both reactant gases are electrochemically consumed, and generate the water and current. In an actual operation, SOFCs are connected in series of multiple cells to increase voltage, thereby obtaining a high output power. An interconnect functions as electrical connectors when the current flows through the cell. The SOFC operation

involves the simultaneous transport of mass, momentum, species and heat which are fully coupled with electrochemical reactions. To comprehend those processes and assist the development of SOFCs technology, numerical simulations based on computational fluid dynamics (CFD) approach are widely used in SOFC research by exploiting the transport phenomena and electrochemical process. CFD simulation is varied upon the research's concerns. Micro-scale model pursues to understand the effect of microstructural properties on the electrochemical characteristics and transport phenomena (Bertei et al. 2013; Costamagna et al. 1998; Chan and Xia 2001; Zhu et al. 2005; Nam and Jeon 2006; Hussain et al. 2006; Kong et al. 2014; Vijay et al. 2017). However, this model is incapable of providing the information in cell-level which is useful in practical application. Macro-scale model deals with physicochemical hydrodynamics in cell- and stack-level and predicts the cell performance with experimentally determined model parameters, but does not pursue the performance prediction in consideration of various microstructures (Achenbach 1994; Nagata et al. 2001; Yakabe et al. 2001; Recknagle et al. 2003; Pramuanjaroenkij et al. 2008; Ni 2012). Recent CFD modeling focuses the development of multi-scale model which in principle combines the advantages of both micro-scale and macro-scale models. Here, we employ the multi-physics and multi-scale model to simulate the SOFC operation.

Recently, the cell-level SOFC model on the open-source software is developed by the author and co-workers (Beale et al. 2016; Jeon 2019). The work was originated from the Multi-Scale Integrated Fuel Cell Model (MUSIC) program, in which the goal is to develop a fully-integrated multi-scale fuel cell modeling capability, from micro-scale through to cell, stack, and 'hotbox' levels. We select the object-oriented CFD code, Open Field Operation and Manipulation (OpenFOAM) (http://www.openfoam.com), as a development platform and released the source code on the internet (http://openfuelcell.sourceforge.net). The public availability of open-source fuel cell code, openFuelCell, has stimulated the activities of code development (Beale et al. 2011, 2018; Nishida et al. 2018) and application to other types of fuel cell (Kone et al. 2018; Zhang et al. 2018). The openFuelCell is a multi-physics and multi-scale model that the users easily access the source code and free to modify the code as desired. The model describes complex transport and electrochemical phenomena in a variety of geometrical configurations. This model enables to deal with multiple regions within a single solver, with efficient data transfer between them. Each region supports its own set of fields such as pressure, velocity, concentration and temperature, with associated boundary conditions, while computational domain is decomposed into several regions. Validation and verification activities have been carried out under the program of the International Energy Agency Advanced Fuel Cells Implementing Agreement (IEA AFCIA) (Nishida et al. 2018; Le et al. 2015). However SOFC modeling with openFuelCell has several challenges, such as limited application to planar configuration, unavailability of internal reforming process, high-calculation cost, etc. The present software extends the capability to simulate the stack model.

In this chapter, we introduce the open-source SOFC model which is developed with OpenFOAM®. The widely used anode-supported SOFC is chosen to describe the modeling process. The details of SOFC modeling are described in each section: model

equations in Sect. 2; numerical implementation including calculation procedure in Sect. 3; model description including geometry, mesh and boundary condition in Sect. 4; results and discussion in Sect. 5.

2 Model Equations

2.1 *Governing Equations*

CFD model simulates the heat and mass transfer phenomena in SOFCs. The multi-scale and complex transport phenomena are based on the coupled set of conservation equations of mass, momentum, species transport and energy. The conservation of mass can be expressed in the form of the steady-state equation of continuity:

$$\text{div}\left(\rho \vec{u}\right) = S_m \tag{1}$$

$$S_m = \sum_{i=1}^{n} S_i \tag{2}$$

where the source terms are in general non-zero as a result of production of water and consumption of hydrogen and oxygen caused by electrochemical reactions. The conservation of linear momentum for steady-state flow in the absence of external body forces yields:

$$\text{div}\left(\rho \vec{u} \cdot \vec{u}\right) = -\text{grad}\, P + \text{div}\left(\mu \text{grad}\,\vec{u}\right) + S_p \tag{3}$$

$$S_p = -\frac{\mu \vec{u}}{K} \tag{4}$$

where the source term on the right hand side of the equation is only added in the porous regions such that neglecting the convection and viscous terms in Eq. (3) yields conservation of linear momentum expressed in the form of Darcy's law. Using the generalized Fick's law and neglecting the thermal-diffusion (Soret) effect, the conservation of species mass yields:

$$\text{div}\left(\rho \vec{u}\, y_i\right) = \text{div}\left(D_i^{eff} \text{grad}\, y_i\right) + S_i \tag{5}$$

$$S_{H_2} = -\frac{i}{2F} M_{H_2},\ S_{H_2O} = \frac{i}{2F} M_{H_2O},\ S_{O_2} = -\frac{i}{4F} M_{O_2} \tag{6}$$

where the effective Fick diffusion coefficients are given in terms of values at reference pressure and temperature. Neglecting kinetic energy convection, viscous dissipation, and the diffusion–thermo (Dufour) effect, conservation of energy for steady-state flow yields:

$$\text{div}\left(\rho C_p \overrightarrow{u} \, T\right) - \text{div}(k \text{gradT}) = S_h^e + S_h^j \tag{7}$$

$$S_h^e = \frac{i}{2F}\Delta H(T) - i V^{cell}, \ S_h^j = i^2 R \tag{8}$$

where the source term takes into account local heat production due to joule heating and reversible enthalpy changes. More detailed description for the equations can be found in Beale et al. (2016) and Jeon (2019).

2.2 Electrochemical Model

The electrochemical model determines the current density and overpotentials at a given cell voltage. The cell voltage V^{cell} is calculated as the combination of open circuit voltage (OCV) V^{OCV}, anode activation overpotential η_A^{act}, cathode activation overpotential η_C^{act}, anode concentration overpotential η_A^{conc}, cathode concentration overpotential η_C^{conc}, and electrolyte overpotential (i.e., ohmic loss in electrolyte), η_E, as

$$V^{cell} = V^{OCV} - \eta_A^{act} - \eta_C^{act} - \eta_A^{conc} - \eta_C^{conc} - \eta_E \tag{9}$$

$$V^{OCV} = -\frac{\Delta G^0}{2F} + \frac{R_g T}{2F} ln\left(\frac{x_{H_2}}{x_{H_2O}}\left(x_{O_2}\right)^{\frac{1}{2}}\right) \tag{10}$$

To calculate the activation overpotential η^{act}, the Butler-Volmer expression can be used to describe $\eta^{act} - i$ relationships

$$i = i_0\left[exp\left(\frac{\alpha_a F \eta^{act}}{R_g T}\right) - exp\left(-\frac{\alpha_c F \eta^{act}}{R_g T}\right)\right] \tag{11}$$

where i_0 is the exchange current density, α_a and α_c are the anodic and cathodic charge transfer coefficient, respectively. To determine the concentration overpotential η_C, the following equations can be used:

$$\eta_A^{conc} = -\frac{R_g T}{2F} ln\left(\frac{P_{H_2}}{P_{H_2}^0}\frac{P_{H_2O}^0}{P_{H_2O}}\right) \tag{12}$$

$$\eta_C^{conc} = -\frac{R_g T}{4F} ln\left(\frac{P_{O_2}}{P_{O_2}^0}\right) \tag{13}$$

where P_i^0 is an inlet pressure of species i. However, concentration overpotential can be neglected if the porous media transport and electrochemical reactions are modeled in detail (Janardhanan and Deutschmann 2006). The electrolyte overpotential η_E is dependent on the current density, electrolyte thickness, and temperature which are obtained by

$$\eta_E = \frac{i l_E}{\sigma_E} \tag{14}$$

where l_E is electrolyte thickness, σ_E is electrolyte conductivity.

3 Numerical Implementation

OpenFOAM® solves a set of governing equations using a finite volume scheme written in programming language C++. The main components are: (1) Second order finite volume discretisation on three-dimensional meshes, with polyhedral cell support and capability of handling local mesh refinement, (2) Versatile and transparent representation of partial differential equations in the code, achieved through equation mimicking, (3) A complete set of implicit discretisation operators, and associated matrix and linear solver classes, (4) Massive parallelisation in domain decomposition mode, (5) The capability of dealing with multiple overlapping regions within a single solver, with efficient data transfer between them. Each region can support its own set of fields, e.g., pressure, velocity, species concentration, energy, with associated boundary conditions, (6) Access to libraries of real material properties for single species and their mixtures, (7) Efficient and validated set of heat transfer, fluid flow, chemical reaction, and electrochemistry solvers.

The pressure-momentum coupling is solved using the Pressure Implicit with Splitting of Operators (PISO) algorithm. Linear algebraic systems are solved using Preconditioned bi-conjugate gradient (PBiCG) solver with Diagonal-based Incomplete LU (DILU) preconditioner for velocity, mass fraction, and temperature, and Preconditioned conjugate gradient (PCG) solver with Diagonal-based Incomplete Cholesky (DIC) preconditioner for pressure. Volumetric equations are discretized on the fixed and structured meshes composed of hexahedral element. Three-dimensional (3D) mesh is generated using automatic meshing technique. The meshes are composed of global-region and sub-regions which are split up into individual components. The continuity, momentum and species transport equations are solved on the individual meshes, while energy equation is solved on the global mesh. The calculated properties and variables are passed back and forth between global and

individual meshes by mapping function. The physical properties of gases are calculated by accessing to OpenFOAM® library or class library. The solution algorithm proceeds as follows:

1. Create the cell geometry, specify boundary conditions, assign physical properties, and prescribe average current density.
2. Calculate continuity and momentum equation.
3. Calculate Nernst potential, overpotentials, and cell voltage.
4. Calculate sources of mass, species, and energy.
5. Calculate conservation equations of species transport and energy.
6. Repeat steps (2)–(5) until convergence is obtained.

The algorithm is sequential and iterative. The cell voltage is computed by prescribing a designed current density i^{des} as

$$V^{cell} + = \alpha \times (\bar{i} - i^{des}) \tag{15}$$

where α is a relaxation factor. The calculations are repeated until the difference between the computed mean current density $\bar{i}$ and designed current density i^{des} is within the convergence criteria.

4 Geometry, Mesh and Boundary Condition

For an application, a planar-type anode-supported SOFC is modeled as shown in Fig. 1. The basic unit is composed of interconnects, gas channels, and PEN. The flow channels are embedded within the rectangular cross-section of interconnects. The fuel and air channels are separated by PEN which is composed of five layers: (1) anode substrate layer (ASL), (2) anode functional layer (AFL), (3) electrolyte, (4) cathode functional layer (CFL), and (5) cathode current collector layer (CCCL). Large-scale anode-supported SOFC is modeled that has reaction area of 100 cm^2 (10 cm × 10 cm) and channel size of 1 mm × 1 mm with same rib-spacing width as channel width. Co-flow configuration is considered. Through the grid independency test, total mesh of 2.08 million is used for the simulation (Fig. 2). The finer mesh increase the accuracy, but incurs high calculation cost. Neumann boundary condition is applied on the wall boundaries (adiabatic), and Dirichlet boundary condition is imposed on the inlet, top and bottom boundaries (constant temperature).

The cell geometry can be constructed using commercial software or can be virtually generated using numerical algorithm. Here, we create a geometry and mesh the entire domain using the mesh generation utility *blockMesh* and the geometry generation utility *cellSets*. A directory file named *blockMeshDict* located in the run/constant/polymesh directory. The *blockMesh* reads this dictionary, and writes out the mesh data to *points* and *faces*, *cells* and *boundary* files in the same directory.
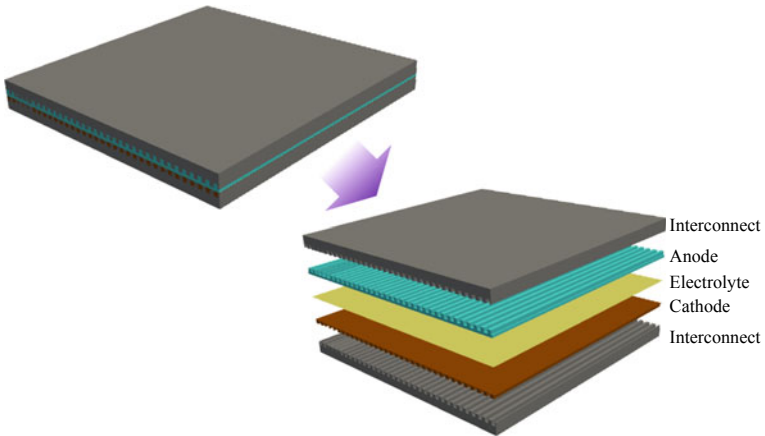
Fig. 1 Schematic diagram of planar-type anode-supported SOFC. Computational domain includes interconnects, channels, anode, electrolyte and cathode. Reproduced from Jeon (2019) with permission from Elsevier
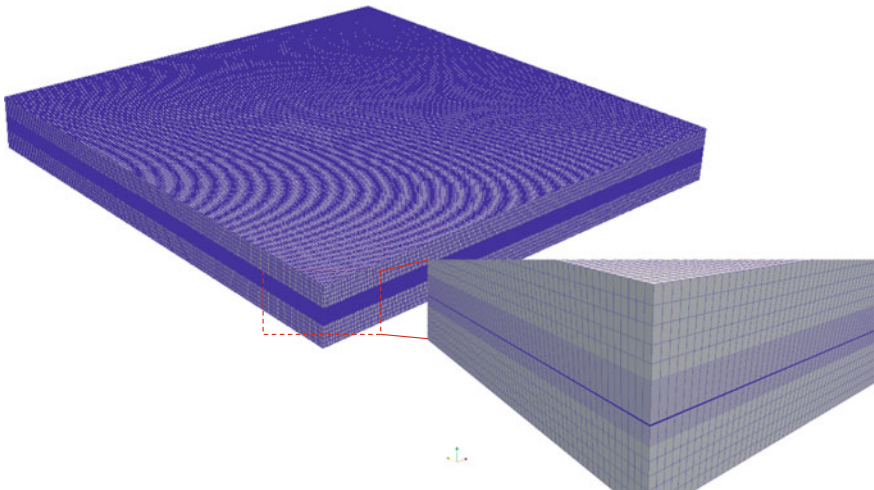

Fig. 2 Tessellated meshes for a planar-type anode-supported SOFC. The zoom-in view illustrates the structured-rectangular meshes

The *cellSets* makes up the cells of each region, and generate the meshes for each region. The *cellSets* for the regions are specified in /run/config directory.

5 Results and Discussion

This section discusses the computed results of anode-supported SOFCs. Geometry details, cell properties and operating condition that used in simulation are listed in Table 1. The user can visualize the results using the post-processing tool, such as *ParaView* and *EnSight*.

In this simulation, we employed the most common choice materials for SOFC components, which are yittria stabilized zirconia (YSZ) for electrolyte, Ni–YSZ cermet for anode, and lanthanum strontium manganite (LSM)–YSZ cermet for cathode. To calculate the activation overpotential η^{act}, the modified Butler-Volmer expression which is taken from Janardhanan and Deutschmann (2006) and Zhu et al. (2005) is used as.

$$i_A = i_{0,A}\left[exp\left(\frac{(\beta_a+1)F\eta_A^{act}}{R_g T}\right) - exp\left(\frac{\beta_c F\eta_A^{act}}{R_g T}\right)\right] \tag{16}$$

$$i_{0,A} = i_{H2}^*\left[\frac{(P_{H2}/P_{H2}^*)^{1/4}(P_{H2O})^{3/4}}{1+(P_{H2}/P_{H2}^*)}\right] \tag{17}$$

$$i_{H2}^* = K_{H2}exp\left(-\frac{E_{H2}}{RT}\right) \tag{18}$$

$$P_{H2}^* = \frac{A_{des}\Gamma^2\sqrt{2\pi R T M_{H2}}}{\gamma_0}exp\left(-\frac{E_{des}}{R_g T}\right) \tag{19}$$

where $\beta_c = 0.5$, $\beta_a + \beta_c = 1$, $K_{H2} = 2.07 \times 10^5 Am^{-2}$ and $E_{H2} = 87.8KJmol^{-1}$. The pre-exponent factor $A_{des} = 5.59 \times 10^9 scm^2mol^{-1}$, the surface site density $\Gamma = 2.6 \times 10^{-9} molcm^{-2}$, the activation energy $E_{des} = 88.12KJmol^{-1}$, and the

Table 1 Properties and operating conditions

Properties						
	l (μm)	d_p (μm)	ε	τ	κ (W/m k)	C_p (J/kg·K)
ASL	1000	2	0.5	3	3	1000
AFL	20	1	0.25			
Electrolyte	10	–	–	–	2.4	550
CLF	20	1	0.25	3	3	750
CCCL	50	6	0.5			
Interconnect	5000	–	–	–	24	660
Operating conditions						
$x_{H_2}^o$, $x_{O_2}^o$	0.97, 0.21					
u_{fuel}, u_{air}	1 m/s, 2 m/s					

sticking probability $\gamma_0 = 0.01$.

$$i_C = i_{0,C}\left[exp\left(\frac{\beta_a F \eta_C^{act}}{R_g T}\right) - exp\left(\frac{\beta_C F \eta_C^{act}}{R_g T}\right)\right] \tag{20}$$

$$i_{0,C} = i_{O2}^* \frac{\left(P_{O2}/P_{O2}^*\right)^{1/4}}{1 + \left(P_{O2}/P_{O2}^*\right)^{1/2}} \tag{21}$$

$$i_{O2}^* = K_{O2} exp\left(-\frac{E_{O2}}{R_g T}\right) \tag{22}$$

$$P_{O2}^* = A_{O2} exp\left(-\frac{E_{O2}}{R_g T}\right) \tag{23}$$

where $K_{O2} = 5.19 \times 10^4 Am^{-2}$, $E_{O2} = 88.6 KJmol^{-1}$, $A_{O2} = 4.9 \times 10^8 atm$ and $E_{O2} = 200 KJmol^{-1}$. Note that Butler-Volmer expression established by Janardhanan and Deutschmann (2006) was modified at the temperature range of 600 – 800 °C. The electrolyte conductivity of YSZ which are obtained by Ferguson et al. (1996) is

$$\sigma_E = 3.34 \times 10^4 exp\left(-\frac{10300}{T}\right) \tag{24}$$

Figure 3 shows the simulated performance with contribution of component overpotentials at 700 °C. The performance decreases as the current density increases. The contributions of anode overpotential and cathode overpotential are large at low current density, but the contribution of cathode overpotential becomes dominant at high current density. The contribution of electrolyte overpotential is not significant which is generally large during the SOFC operation. This is mainly attributed to thin electrolyte layer.

The simulated result also provides the detailed information for dependent variables. Figure 4 shows illustrative examples of the distributions of current density, temperature, species mass fraction and component overpotential at 700 °C. As shown, current density is high at the inlet where the mole fraction of reactants is high, and becomes lower along the electrode length. Current density distribution affects temperature distribution which is high at the inlet and low at the outlet. The mole fractions of hydrogen and oxygen are high at the inlet, and becomes lower along the electrode length. Hence, activation overpotentials are high at the inlet, and concentration overpotentials are high at the outlet. Interestingly, several straight lines are observed all the figures likely due to non-uniform electrochemical reaction. This is ascribed to non-uniform oxygen distribution, in which oxygen mole fraction is observed high at the channel area, but low at the rib area. These severely non-uniform distributions are attributed to the thin cathode layer. To avoid non-uniform distributions,
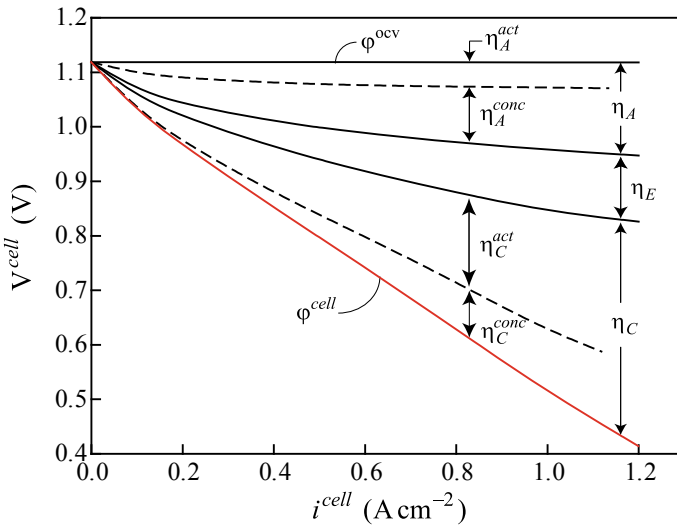
Fig. 3 Simulated performance and contribution of component overpotentials to the overall potential loss of anode-supported SOFC at 700 °C. Reproduced from Jeon (2019) with permission from Elsevier

blowing the air with high stoichiometric flow rate or optimum design of cathode microstructure is desirable (Fig. 5).

Oxygen depletion during calculation

When operating anode-supported SOFC, the oxygen can be depleted at high current densities. Although the actual SOFC can operate regardless depletion, the model calculation will fail to converge. Once the oxidant is starved, the mole fraction of oxygen gets zero or negative value that affects the calculation of concentration overpotential in Equation 26, resulting in mathematical error. This typically occurs under the rib where the oxidant is difficult to reach due to thin cathode layer, as seen in Figure 5. To avoid this type of calculation failure, zero or negative mole fractions must be replaced to small positive number. Slow converging with low relaxation factor will also be helpful.
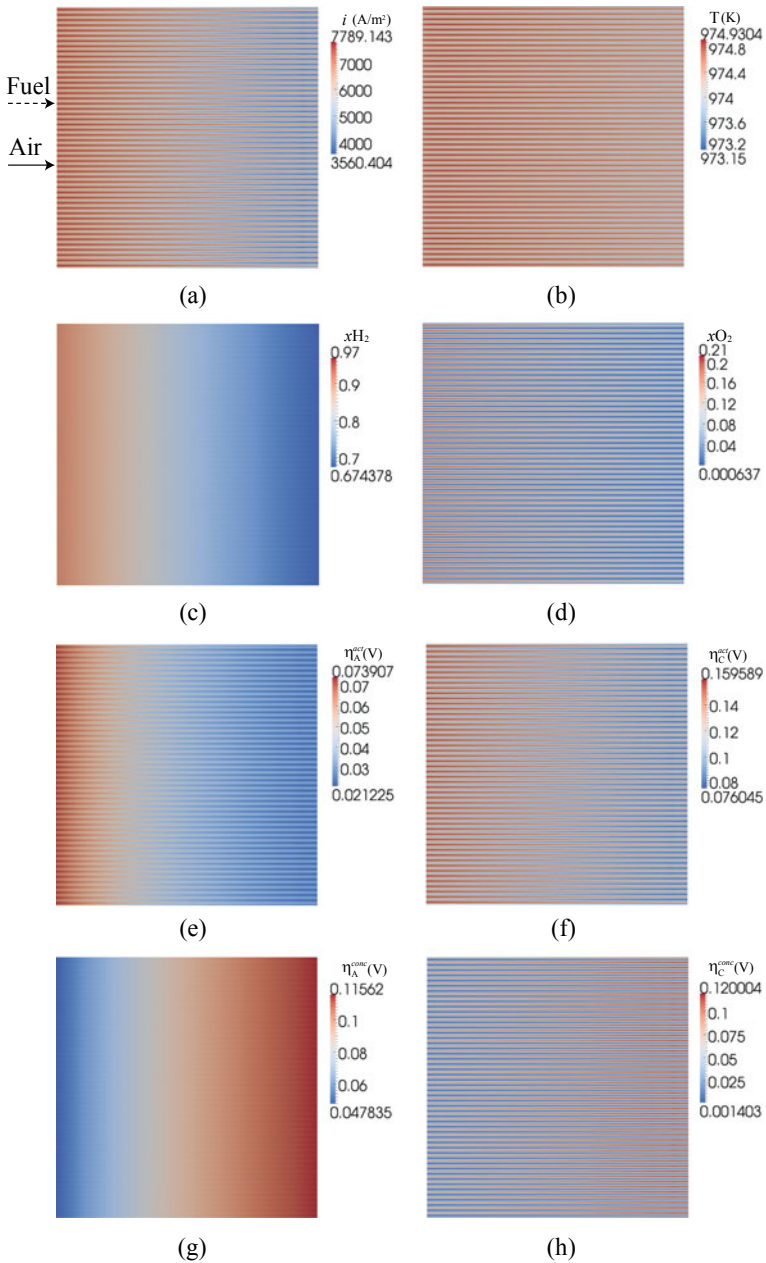
Fig. 4 Distributions of **a** current density, **b** temperature, **c** hydrogen mole fraction, **d** oxygen mole fraction, **e** anode activation overpotential, **f** cathode activation overpotential, **g** anode concentration overpotential and **h** cathode concentration overpotential on electrode surfaces at 0.6 A/cm^2 and 700 °C. Reproduced from Jeon (2019) with permission from Elsevier

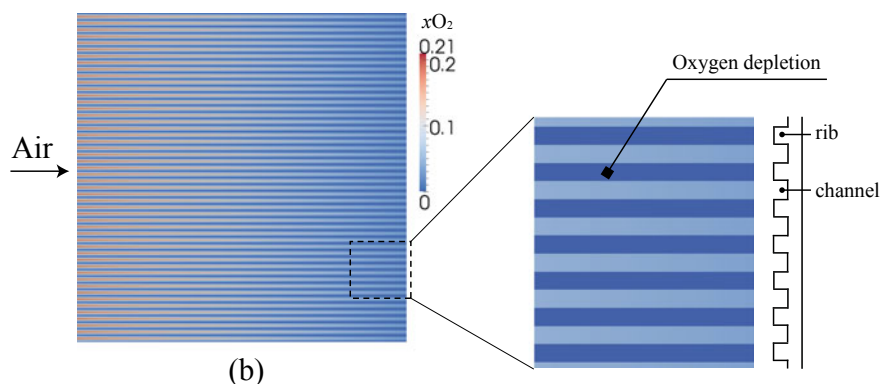**Fig. 5** Oxygen mole fraction distributions on CFL surface at 1.0 A/cm^2 and 700 °C. Reproduced from Jeon (2019) with permission from Elsevier

References

Achenbach E (1994) Three-dimensional and time-dependent simulation of a planar solid oxide fuel cell stack. J Power Sour 49:333–348

Beale SB, Le AD, Roth HK, Pharoah JG, Choi H-W, de Haart LGJ, Froning D (2011) Numerical and experimental analysis of a solid oxide fuel cell stack. ECS Trans 35(1):935–943

Beale S, Choi H-W, Pharoah JG, Roth HK, Jasak H, Jeon DH (2016) Open-source computational model of a solid oxide fuel cell. Comp Phys Commu 200:15–26

Beale SB, Reimer U, Froningm D, Jasak H, Andersson M, Pharoah JG, Lehnert W (2018) Stability issues of fuel cell models in the activation and concentration regimes. J Electrochem Energy Conv Storage 15:041008

Bertei A, Nucci B, Nicolella C (2013) Microstructure modeling for prediction of transport properties and electrochemical performance in SOFC composite electrodes. Chem Eng Sci 101:175–190

Chan SH, Xia ZT (2001) Anode micro model of solid oxide fuel cell. J Electrochem Soc 148:A388–A394

Costamagna P, Costa P, Antonucci V (1998) Micro-modelling of solid oxide fuel cell electrodes. Electrochim Acta 43:375–394

Ferguson JR, Fiard JM, Herbin R (1996) Three-dimensional numerical simulation for various geometries of solid oxide fuel cells. J Power Sources 58:109–122

Hajimolana SA, Hussain MA, Ashri Wan Daud WM, Soroush M, Shamiri A (2011) Mathematical modeling of solid oxide fuel cells: a review. Renew Sust Energy Rev 15:1893–1917

Hussain MM, Li X, Dincer I (2006) Mathematical modeling of planar solid oxide fuel cell. J Power Sour 161:1012–1022

Janardhanan VM, Deutschmann O (2006) CFD analysis of a solid oxide fuel cell with internal reforming: Coupled interactions of transport, heterogeneous catalysis and electrochemical processes. J Power Sources 162:1192–1202

Jeon DH (2019) Computational fluid dynamics simulation of anode-supported solid oxide fuel cells with implementing complete overpotential model. Energy 188:116050

Kone J-P, Zhang X, Yan Y, Hu G, Ahmadi G (2018) CFD modeling and simulation of PEM fuel cell using OpenFOAM. Energy Procedia 145:64–69

Kong W, Gao X, Liu S, Su S, Chen D (2014) Optimization of the interconnect ribs for a cathode-supported solid oxide fuel cell. Energies 7:295–313

Le AD, Beale SB, Pharoah JG (2015) Validation of a solid oxide fuel cell model on the international energy agency benchmark case with hydrogen fuel. Fuel Cells 15:27–41

Nagata S, Momma A, Kato T, Kasuga Y (2001) Numerical analysis of output characteristics of tubular SOFC with internal reformer. J Power Sour 101:60–71

Nam JH, Jeon DH (2006) A comprehensive micro-scale model for transport and reaction in intermediate temperature solid oxide fuel cell. Electrochim Acta 51:3446–3460

Ni M (2012) Modeling of SOFC running on partially pre-reformed gas mixture. Intl J Hydrog Energy 37:1731–1745

Nishida RT, Beale SB, Pharoah JG, de Haart LGJ, Blum L (2018) Three-dimensional modelling and experimental validation of the Julich Mark-F solid oxide fuel cells. J Power Sour 373:203–210

OpenFOAM®: the open source CFD toolbox available from http://www.openfoam.com

Pramuanjaroenkij A, Kakac S, Zhou XY (2008) Mathematical analysis of planar solid oxide fuel cells. Intl J Hydrog Energy 33:2547–2565

Recknagle KP, Williford RE, Chick LA, Rector DR, Khaleel MA (2003) Three-dimensional thermos-fluid electrochemical modeling of planar SOFC stacks. J Power Sour 113:109–114

Vijay P, Tade MO, Shao Z, Ni M (2017) Modelling the triple phase boundary length in infiltrated SOFC electrodes. Intl J Hydrog Energy 42:28836–28851

Yakabe H, Ogiwara T, Hishinuma M, Yasuda I (2001) 3-D model calculation for planar SOFC. J Power Sour 102:144–154

Zhang S, Reimer U, Beale SB, Lehnert W, Stolten D (2018) Modeling polymer electrolyte fuel cells: a high precision analysis. Appl Energy 233–234:1094–1103

Zhu H, Kee RJ, Janardhanan VM, Deutschmann O, Goodwin DG (2005) Modeling elementary heterogeneous chemistry and electrochemistry in solid-oxide fuel cells. J Electrochem Soc 152:A2427–A2440